# Physics-Aware Processing of Rotational Micro-Doppler Signatures for DBN-Based UAS Classification Radar

Arjuna Madanayake\*, Gihan J. Mendis †, Viduneth Ariyarathna \*, Sravan Pulipati \*, Tharindu Randeny ‡, Shubhendu Bhardwaj \*, Xin Wang §, Soumyajit Mandal ¶ and Jin Wei †

\*Department of Electrical and Computer Engineering, Florida International University, Miami, FL, USA † Department of Computer and Information Technology, Purdue University, West Lafayette, IN, USA ‡ Department of Electrical and Computer Engineering, University of Akron, OH, USA §Department of Electrical and Computer Engineering, Stony Brook University, Stony Brook, NY, USA ¶Department of Electrical and Computer Engineering, University of Florida, Gainesville, FL, USA Email: amadanay@fiu.edu

Abstract—This paper describes hardware, signal processing, and machine learning methods for Doppler radar-based accurate and robust detection of micro unmanned aerial systems (UAS). Typical detection accuracy of  ${\sim}98\%$  was obtained in over-the-air tests with a 2.4 GHz continuous wave (CW) radar and a variety of commercially-available micro-UAS devices. Several methods are described for further improving detection performance, including multi-beam synthesis with uniform circular arrays to provide 360° azimuthal sensitivity; dielectric lens antennas and focal plane arrays at mm-wave frequencies (28 GHz) for improved spatial resolution; and polyspectra-based feature extraction methods for improved modeling of nonlinear phase modulation processes within the measured Doppler signatures.

#### I. Introduction

Remotely-piloted or self-piloted micro unmanned aerial systems (UAS) are everywhere. Commonly known as "drones" by the general public, micro UAS have become a rapidly growing area of development for 5G/6G wireless communications, wireless Internet of Things (IoT), aerial robotics, and surveillance/security [1]-[4]. The low cost and mass producible nature of micro UAS has led to a plethora of applications making UAS one of the most exciting and exponentially growing sectors in aerospace and wireless engineering in modern times. However, like many high technologies, micro UAS can be highly dangerous when used by bad actors [5]-[8]. One of the most pressing problems in today's war on terror is the increasing use of micro UAS as weapons. An improvised explosive device (IED) or biological weapon can wreak havoc in the community when UAS are used as vectors for clandestine transportation.

The problem is detecting an unauthorized micro-UAS can be addressed using two approaches: 1) detection of the wireless remote control signal [9], [10], and 2) detection of the UAS itself using physical methods [11]–[16]. In our work, we explore the latter because the real danger lies in automated flight controller-based micro-UAS that have no detectable wireless signal as there exists no need for a human pilot. In

978-1-7281-5576-0/20/\$31.00 ©2020 IEEE

such situations, the UAS must be detected using its physical interaction with the environment. Examples include optical detection using a camera, audio detection, and radio detection using radar techniques. Optical- and audio-based detection is unreliable in cloudy/smoky and loud environments, which would be the norm in conflict situations. Therefore, one must resort to electromagnetic signatures for reliable detection at sufficiently long distances. The primary approach that is pursued here is to exploit the repeating "chopping" of a radar interrogation signal by the rotors of a UAS as a method for identifying a unique signature that can classify different types of UAS as well as different types of motion. In our previous work, we developed deep learning approaches for single Doppler radar sensor based UAS detection [17]–[19]. In this paper we discuss the use of such rotational micro-Doppler signatures for UAS type detection with improvements including multi-beam synthesis with uniform circular arrays, dielectric lens antennas and focal plane arrays at mm-wave frequencies (28 GHz), and polyspectra-based feature extraction methods. The possible use of rotational micro-Doppler radar returns for learning the control motions of a UAS that is changing its position is left for another paper.

# II. PHYSICAL ORIGIN OF MICRO-DOPPLER SIGNATURES

When the transmit waveform encounters an UAS, it is subjected to a periodically time-varying radar cross-section due to reflections from the rotors, e.g., the four rotors of a quadcopter. This generates red- and blue-shifted Doppler components in the backscattered rotational micro-Doppler signal. The spectra of these signals was experimentally analyzed using standard FFT-based DSP algorithms. They were found to depend on several physical parameters, so that the radar return is approximately

$$x(t) = \sum_{k=1}^{M} \cos\left(\omega t + f_k(r_k, \dot{\theta_k}, x_k, y_k)\right) \tag{1}$$

for k=1,2,...M. These parameters include i) carrier frequency  $\omega=2\pi f_c$ , ii) number of rotors M, iii) orientation of the rotor with respect to the incident signal, iv) speed of rotation  $\theta_k$ , v) number of blades per rotor  $N_k$ , vi) relative directions of rotation of multiple rotors, and vii) the relative size of each rotor  $(d_k=2r_k)$  compared to the radar wavelength  $\lambda=cf_c$ , where c is the speed of light.

The phase modulation of x(t) is governed by the modulation functions  $f_k(\cdot)$ . In the simplest quadrotor case (M=4 and N=2) where  $\lambda\gg d$ , the reflected signal is phase-modulated with a low modulation index, resulting in two sidebands (red and blue shifted). In practice,  $\lambda\sim d$ , making the phase modulation strongly non-linear. Several algorithms can be used to extract uniquely identifiable signatures from these modulated signals. These include the DFT, the power spectrum density (PSD), and higher-order statistical techniques. In particular, the spectral correlation function (SCF), which is an optimum algorithm for extracting signatures from cyclostationary signals, can be used as a pre-processing step.

# III. MICRO-UAS DETECTION AND IDENTIFICATION

#### A. SCF-based Feature Extraction

The cyclic autocorrelation function (CAF) can quantize the correlation between frequency shifted versions of a given signal and represents the fundamental parameters of any second-order periodicity [20], [21]. Let  $T_0$  be the process period and let  $\alpha = \frac{\hat{m}}{T_0}$  be the cyclic frequency that indicates the cyclic evolution of the waveforms, where  $\hat{m}$  is an integer; the CAF can be calculated as follows:

$$R_x^{\alpha}[l] = \left[\lim_{N \to \infty} \frac{1}{2N+1} \sum_{n=-N}^{N} x[n] x^*[n-l] e^{-j2\pi\alpha n}\right] e^{-j\pi\alpha l},\tag{2}$$

where  $x[\cdot]$  denotes the rotational micro-Doppler radar return signal, which is modeled by a cyclostationary process. The desired SCF can be calculated by implementing the discrete Fourier transform (DFT) using a fast Fourier transform (FFT) algorithm. The FFT is implemented on  $R_x^{\alpha}$  such that:

$$S_x^{\alpha}[f] = \sum_{l=-\infty}^{\infty} R_x^{\alpha}[l] e^{-j2\pi fl}, \tag{3}$$

where  $R_x^{\alpha}[l]$  is defined in Eq. (2), and f denotes the digital temporal frequency of the radar return signal at baseband. Typically, we expect the rotational micro-Doppler signals to have less than 10 kHz of bandwidth.

The two-dimensional (2-D) SCF output matrix (i.e., image/pattern) can be obtained by calculating Eq. (3) for different values of  $\alpha$  and f. For practical implementations, it is not possible to consider an infinite number of samples; however, we use the largest possible number of samples. In our current implementations, N in Eq. (2) is limited to 2048, l is considered to be an integer and within the range of [-1024,1024], and f in Eq. (3) is the digital frequency in the range of  $[-\pi,\pi]$  with a normalized discrete circular frequency resolution of  $2\pi/2048$  (FFT bin size in rad/sec).

The SCF patterns effectively embody the features of the associated cyclostationary properties even in the presence of high levels of additive white Gaussian noise (AWGN). This is because that AWGN is a stationary process, and thus there are no cyclostationary features in AWGN [21]. In other words, SCF gives good results when a radar return corrupted by AWGN has poor signal-to-noise ratio (SNR).

## B. DBN-based Classifier

The idea is to automate the recognition of each type of UAS based on its unique rotational micro-Doppler radar return by using the SCF as a pre-processing step. Ideally, the SCF generates a unique output image depending on the physics of the UAS rotational micro-Doppler return, thus enabling reliable recognition. Various machine learning algorithms have been tried for this purpose, and it has become apparent that the deep learning approach gives the best results for our particular set of test cases. The fact that deep learning happens to give the best results is based on experimental observation. It has not be proven mathematically as such. Nevertheless, we seek to provide the reader with a summary of our results, as follows.

A deep belief network (DBN) is formed via a stack of restricted Boltzmann machines (RBMs) that in turn are energybased generative stochastic models capable of learning probabilistic distributions of the input data [22]. RBMs consist of a visible layer and a hidden layer of binary units that do not have intra-layer connections [23]. The goal of training RBMs is to learn optimum values for visible-hidden connection weight matrix and biases, such that, the trained RBMs have the ability to probabilistically re-generate inputs from a given set of hidden units. RBMs are trained via the well-known contrastive divergence (CD) unsupervised procedure [24], in which the training method is developed as a gradient-descent method on the negative log-likelihood loss function [25] and then approximated to the CD training [26]. Hidden units of a trained RBM represents abstract features of the input data. However, RBMs are only capable to process binary inputs. SCF signature patterns generated contain real-valued data. Therefore, in order process SCF pattern data, we revise the conventional DBN structure by replacing the first RBM of the DBN with a Gaussian-Bernoulli RBM (GBRBM), which can process real-valued inputs [27].

In order to achieve an effective DBN-based classifier, we first conduct unsupervised training on a stack of RBMs and then place a softmax output layer above the structure. The softmax activation probability for the *j*th output unit can be calculated as follows:

$$P(y=j|\hat{\mathbf{h}}) = \frac{\exp(\mathbf{W}_{j}^{T}\hat{\mathbf{h}})}{\sum_{k=1}^{q} \exp(\mathbf{W}_{k}^{T}\hat{\mathbf{h}})},$$
(4)

where  $\exp(\cdot)$  is an exponential function,  $\hat{\mathbf{h}}$  is the activation vector of the previous hidden layer,  $\mathbf{W_k}$  is the weight vector associated with the connections from the kth output to the

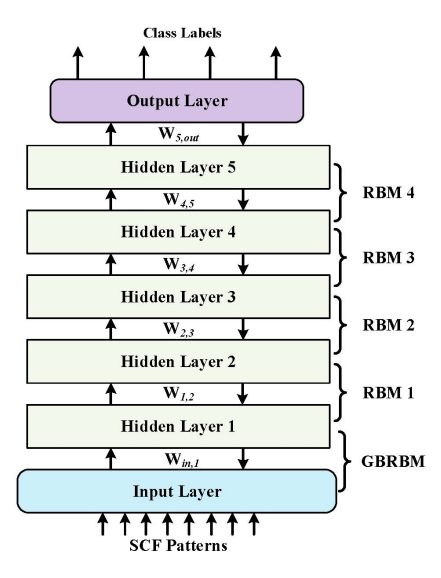


Fig. 1. The DBN-based classifier structure used in the proposed method.

top hidden layer, and q is the number of output units. Using the labeled SCF pattern data, the DBN-based classifier is fine-tuned via the backpropagation supervised training method to act as a classifier [28]. In each iteration of backpropagation supervised training, the actual label of each input SCF pattern is compared with the value predicted by the DBN-based classifier. The achieved prediction error is propagated through the network for updating all the weights and bias parameters. In the backpropagation training of this DBN-based classifier, the initial weights and bias values used are learned from RBM training, which reduces the possibility of the network converging to a local minimum.

#### C. Initial Micro-UAS Experiment Setup

For the initial experiment, we consider a continuous-wave (CW) Doppler radar setup operating on 2.4 GHz with transmit power of 5 dBm. The receiver RF chain consists of a bandpass filter (BPF) having a passband of 2.355 - 2.435 GHz, a low noise amplifier (LNA) with a gain of 48-dB, a downconverting stage, and a low-pass filter (LPF) with a cut-off frequency of 45 MHz. Additionally, LPF with 90 Hz cutoff with analog operational amplifiers with 60 dB gain is used to enhance the Doppler signals related to micro-UAS motion. The Doppler radar setup is implemented in an indoor lab environment. Several commercially-available Micro-UASs are placed in a fixed position with 3m distance from antennas of the Doppler radar setup and the reflected signals are captured and analyzed to characterize the associated SCF signature patterns. Additionally, a reference SCF pattern is generated for the lab environment from the captured signals when there is no UAS in front of the radar sensor.

#### D. Experimental Results

Examples of SCF patterns obtained from several commercially-available UAS the initial radar setup are shown in Fig. 2. The patterns are visually distinct, which is

promising for automated classification. In particular, one can observe a particular pattern for the reference case, i.e., when there are no micro-UASs present in the radar beam. Further, when the radar beam illuminates different micro-UAS, the resulting rotational micro-Doppler returns generate strikingly different-looking SCF images, as visible in the figure. In our hardware implementation, the DBN is trained using 1400 SCF patterns including 200 patterns corresponding to each UAS and the reference. Trained DBNs are tested by using 200 SCF patterns from each category. Table. I shows the confusion matrix for the MATLAB implementation of our DBN-based classifier. In Table I, the rows represent the actual class that each tested SCF pattern belongs to (i.e., the ground truth), while the columns represent the class predicted by the DBN-based classifier.

The detection accuracy as well as the rate of false alarms for the DBN-based classifier have been obtained using the results in Table I. Figs. 3 and 4 show the detection and identification accuracy, respectively. The rate of false positives obtained by the DBN-based classifier was 2%.

Authors would like to mention that this deep learning structure and experimental results were used as a comparison to evaluate a low-complexity hardware-optimized DBN structure in [19].

TABLE I

CLASSIFICATION OF SCF PATTERNS FOR MICRO-UAS DETECTION AND IDENTIFICATION USING A MATLAB IMPLEMENTATION OF A DBN-BASED CLASSIFIER

Actual	Classification from DBN						
Pattern	UAS1	UAS2	UAS3	UAS4	UAS5	UAS6	Ref
UAS1	198	0	2	0	0	0	0
UAS2	5	191	0	1	0	2	1
UAS3	3	6	191	0	0	0	0
UAS4	4	0	5	190	1	0	0
UAS5	0	0	0	0	199	0	1
UAS6	0	0	2	0	1	197	0
Ref	1	0	3	0	0	0	196

### IV. ONGOING WORK

# A. Multi-Directional Situational Awareness at 2.4 GHz

Circular array geometries find applications in micro-UAS detection due to their ability to scan a full  $360^{\circ}$  in the azimuthal plane. The use of circular arrays also enables 2-D beamforming in both azimuthal and elevation planes. Our recent work has focused on digital multi-beam synthesis with N-element uniform circular arrays (UCA) for achieving simultaneous sensitivity over the entire  $360^{\circ}$  range. The digital N-beam generation technique that we propose can generate N equi-spaced beams in the azimuthal plane that can be digitally steered in both elevation and azimuthal planes.

# B. Circular Multibeam Synthesis

A narrowband beam at a direction  $(\phi_{max}, \theta_{max})$  can be generated using an N-element UCA having a radius a. The complex weights  $\alpha_n$  (i.e., phasing factors) needed at each

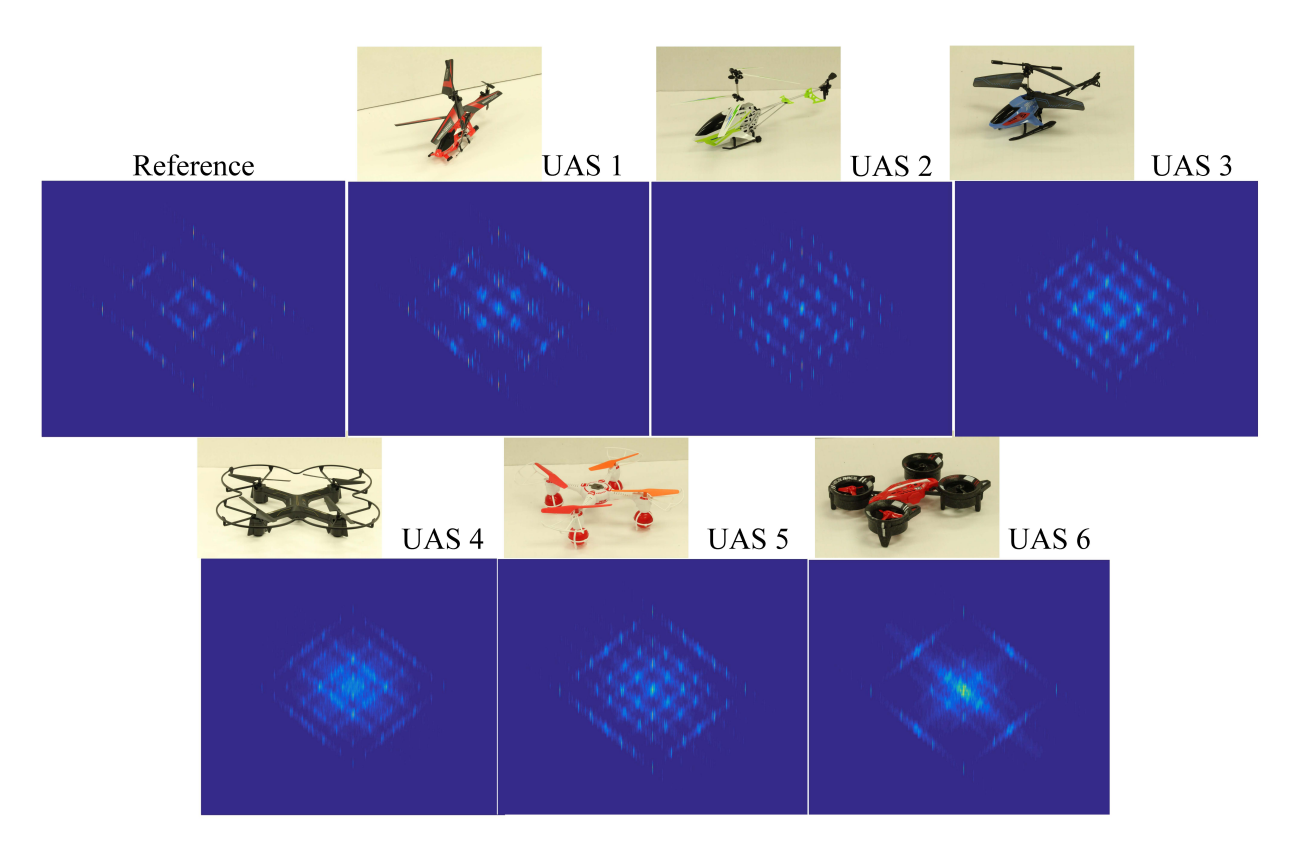


Fig. 2. SCF patterns generated for the reference laboratory environment in the presence of various micro-UASs. In SCF patterns shown in the figure vertical and horizontal axes represent temporal and cyclic frequencies, respectively.

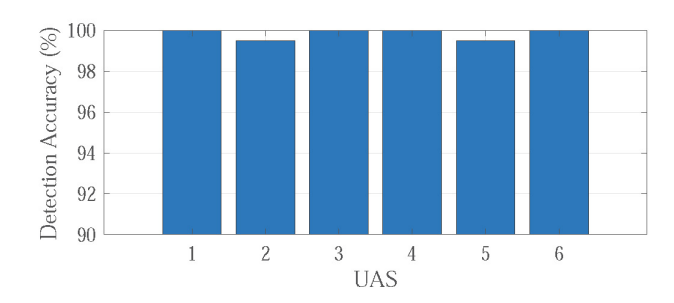


Fig. 3. Accuracy of micro-UAS dectection of DBN based classifier.

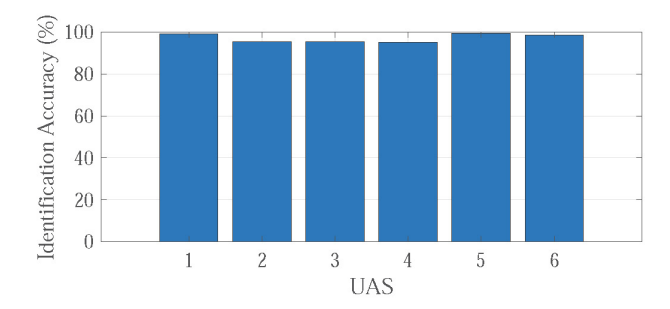


Fig. 4. Accuracy of micro-UAS identification of DBN based classifier.

antenna element to form a beam in the  $(\phi_{max}, \theta_{max})$  direction

are given by [29], [30]

$$\alpha_n = \pm 2m\pi - ka\sin\theta_{max}\cos\left(\phi_{max} - \frac{2\pi n}{N}\right), \quad m \in \mathbb{Z}.$$
(5)

The formation of circular symmetric multibeams requires implementing the beam matrix  $W_N$  given by

$$\mathbf{W}_{N} = \begin{bmatrix} \alpha_{0} & \alpha_{1} & \dots & \alpha_{N-2} & \alpha_{N-1} \\ \alpha_{N-1} & \alpha_{0} & \dots & \alpha_{N-3} & \alpha_{N-2} \\ \vdots & \vdots & \ddots & \vdots & \vdots \\ \alpha_{1} & \alpha_{2} & \dots & \alpha_{N-1} & \alpha_{0} \end{bmatrix} . \tag{6}$$

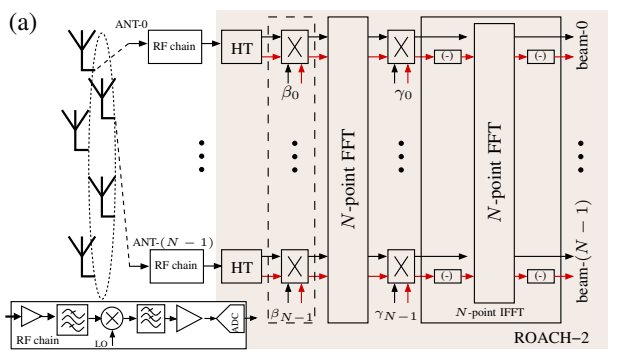
Here,  $\mathbf{W}_N$  takes the form of a circulant matrix. The above computation yields an orthogonal decomposition of  $\mathbf{W}_N$ , i.e.,

$$\mathbf{W}_N = \mathbf{F}_N^{-1} \mathbf{D} \mathbf{F}_N, \tag{7}$$

where  $\mathbf{F}_N$  is the N-point DFT matrix and  $\mathbf{D}$  is a diagonal matrix containing the phased-array coefficients from the original beam generation vector such that  $\mathbf{D} = diag\{\mathcal{F}_N(\mathbf{w})\}$ ; here  $\mathbf{w} = [\alpha_0, \ \alpha_1, \ \dots, \ \alpha_{N-1}]^{\mathsf{T}}$ . Thus, by implementing (7), the complexity of the N-beam computation can be reduced from  $\mathcal{O}(N^2)$  to  $\mathcal{O}(N \log N)$ .

#### C. Hardware Design and Measured Beams

The overall system architecture for realizing (7) digitally is shown in Fig. 5(a). Fig. 5(c) shows the hardware prototype, comprising of a 16-element dipole UCA at 2.4 GHz that



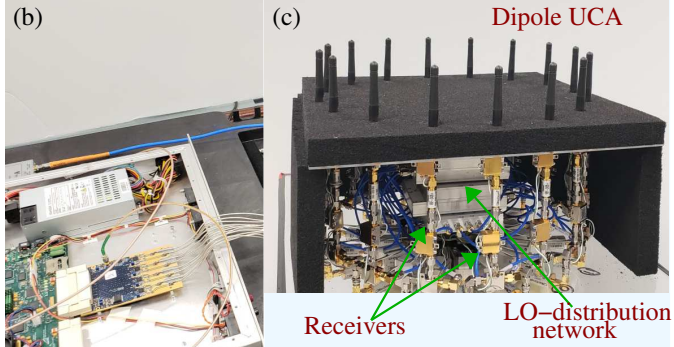


Fig. 5. (a) Overview of the digital realization architecture of the proposed algorithm (block named HT in the diagram refers to Hilbert transform). (b) ROACH-2 digital processing platform that implements the circular *N*-beam computation. (c) 16-element UCA and the RF front-end circuits using commercial off-the-shelf (COTS) electronics.

was custom-built for verifying the circular N-beam algorithm. Fig. 5(b) shows the ROACH-2 field-programmable gate array (FPGA) platform [31] that was used for i) sampling all 16 intermediate frequency (IF) channels, and ii) digital computation of the circular N-beams.

The array front-end supports 100 MHz bandwidth, while the digital back-end can be clocked up to 240 MHz. The circularly-symmetric simultaneous beams generated using the setup were measured in real-time in an open field by using a 2.4 GHz transmitter. The digital coefficients  $\gamma_n$  were set to achieve a maximum sensitivity at  $\theta=70^\circ$  (elevation angle). A transmitter was set approximately in the same elevation with a 4 m separation and beam energy was computed by rotating the receiver array in the azimuthal plane from 0-360°. The measured responses of all 16-beams are shown in Fig. 6.

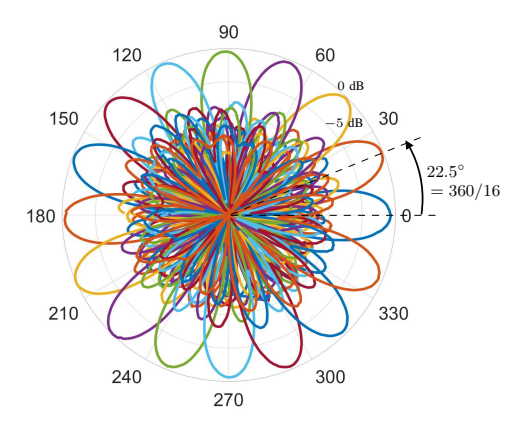


Fig. 6. All 16 measured beams from the prototype UCA.

### D. Multi-Directional Situational Awareness at 28 GHz

Our recent design and implementations of multi-beam digital array receivers has led to ongoing work on fully-digital multi-beam digital array receivers operating at mm-wave for micro-UAS detection, 5G wireless communications, and RF sensing. This ongoing work focuses on sensing with high spatial resolution at 28 GHz using dielectric lens antennas fed

with focal plane array (FPA) feeds that have dedicated 28 GHz receivers at each feed element. Each feed element of the FPA provides a highly-directional far-field RF beam. Several such FPA signals can be combined using focal plane beamforming algorithms, such as the conjugate field matching method which is optimal for AWGN-contaminated radar returns.

Fig. 7(a) shows a typical 28 GHz micro-UAS detection system. Here, the receiver array contains a lens+ 2D FPA architecture to provide very sharp beams that sense and detect the micro-UAS with the help of a similar architecture at transmit side. Since, the operation is at mmWave frequencies, each receiver chain contains a downconversion stage supported by very high amplification stages at back-end as shown in Fig. 7(b). Currently, we developed a 28 GHz digital array receiver as shown in Fig. 7(c) and (d). The dielectric lens antenna was designed and 3D-printed to achieve four independent farfield beams at 28 GHz using a 4-element FPA and set of 4 down-converters. A 4-element patch antenna array, where each patch is built as an 8-element series fed vertical sub-array, serves as the FPA, whereas Analog Devices (HMC1065LP4E) module is employed for down-conversion. Complete details of the antenna array design and receiver setup can be found in [32], [33]. Current experiments have resulted in measured receive-mode RF beams at 28 GHz using the custom-designed lens and FPA system shown in Fig. 8. Ongoing work focuses on transmit-mode 28 GHz lens antenna beamforming and the combination of both multi-beam transmit and receive lens antenna systems for multi-beam MIMO approaches to micro-UAS detection at mm-wave.

The modulation properties of a rotating UAS blade at 28 GHz is expected to be significantly non-linear compared to the same UAS illuminated by a 2.4 GHz or 5.8 GHz waveform. This is because the wavelength at 28 GHz or higher mmwave bands is much smaller than the typical rotor diameter, which makes the phase modulation highly non-linear. The experimental verification of a mathematical model for such mm-wave radar modulation remains an open question.

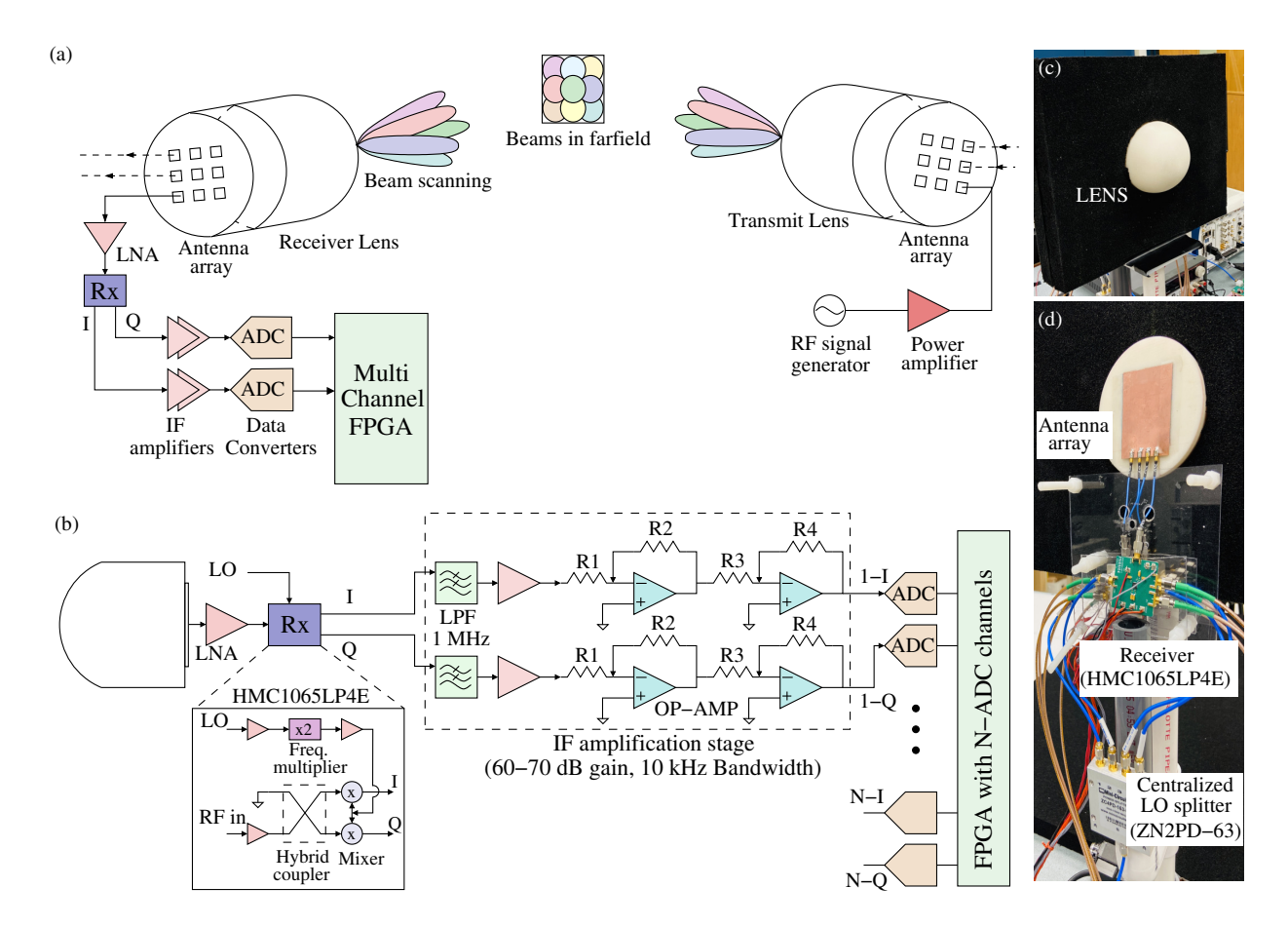


Fig. 7. (a) Overview of a lens based 28 GHz micro-UAS detection system with transmitter on right and receiver on the left. (b) Close up of one receiver chain. (c) Front-view of a lens enclosed in an absorber. (d) A 4-element uniform linear patch array receiver attached to the back of the ABS lens.

# V. ONGOING WORK IN POLYSPECTRA FEATURE EXTRACTION

Currently, we have explored physics-aware modeling of the rotational micro-Doppler signatures, the use of DFT and SCF for extracting recognizable signatures from the received signals, and the use of DBN (and deep CNN)-based machine learning algorithms for classifying the signatures. In ongoing and future work, we are exploring the use of higher-order statistical methods based on the bispectrum and trispectrum [34] that can potentially better extract highly non-linear frequency relationships from the rotational micro-Doppler radar signals at mm-wave bands [35]. Such highly non-linear frequency relationships in the rotational micro-Doppler Doppler backscatter are expected when the RF carrier wavelength is much shorter than the dimensions of the UAS rotors: for example, when using mm-wave radar beams for detecting and identifying micro-UAS (e.g., a typical hexacopter with 30 cm blades being interrogated with 77 GHz "automotive" radar).

The linear transform based DFT leads to the straightforward computation of the power spectrum (PS) of the signal, which is based on autocorrelation properties. However, the PS estimation considers the process under consideration a superposition of statistically uncorrelated harmonic (i.e., Fourier) compo-

nents. Therefore, only linear physics processes governing the process can be captured using a purely DFT (and therefore, PS based) methods. In real-world mm-wave Doppler radar, highly non-linear physics causes multiple highly phase-correlated spectral components that must be efficiently detected as part of baking in the physics of such non-linear effects into a deep learning or other machine learning model. The use of higher-order statistical methods leads to polyspectrum based digital signal processing (PDSP), which can extract the correlated phase relationships that may exist between frequency components. PDSP techniques can also capture the possible non-Gaussian nature of the mm-wave micro-UAS rotational Doppler return signal [36].

Higher order spectra (that is, the so-called polyspectum) are defined in terms of the higher order cumulants of the underlying process. The third-order spectrum, known as bispectrum, and the fourth-order spectrum, known as trispectrum, can extract quadratic and cubic non-linearity from the underlying process. Using both bispectrum and trispectrum as a pre-processing step before machine learning algorithms can allow for the efficient recognition of quadratic and cubic non-linearity arising from the physics of the UAS rotors chopping a high-frequency RF carrier (28, 60, 77, 94 GHz etc.,) better than

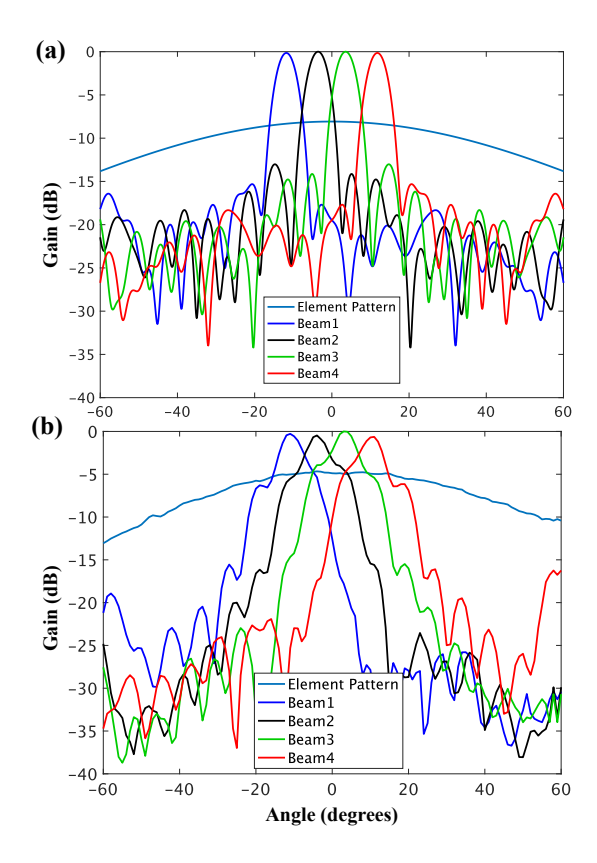


Fig. 8. (a) Normalized beam patterns simulated in CST. Elemental sub-array gain pattern (normalized by the maximum of beam pattern) is shown for comparison. (b) Measured normalized beam patterns using the 28 GHz lens array setup and corresponding normalized elemental subarray pattern.

linear DFT-based methods. The comparison of the bispectrum and trispectrum with the SCF is also of interest, since the SCF does contain higher-order statistical information.

Thus, the use of PDSP as a pre-processing step before machine learning achieves several important advantages: 1) optimal extraction of information due to deviation from Gaussianness (normality); 2) estimation and recognition of phase relationships between non-Gaussian parametric signals, such as the frequency components of rotational micro-Doppler UAS radar return signals [37]; and 3) detection, characterization, and recognition of the non-linear properties of underlying physical mechanisms (rotor size, number of blades, rotor orientation, rotational speeds, relative position, RF carrier wavelength, polarization etc.). The rotational nature of the physics of the UAS rotors is a good example of how an UAS can generate a non-Gaussian radar return, which can become either periodic or quasi-periodic as the UAS hovers at a set location or changes its position/correcting attitude/altitude.

Apart from tracking the non-linear phase relationships between the frequency components of micro-Doppler returns, the use of PDSP [37] is also expected to facilitate machine learning algorithms for recognizing both UAS type as well as various control functions for each type (i.e., motion sequence M for a type-N UAS, which is "left lift and move up").

PDSP also preserves the phase of non-Gaussian parametric signals [37], which may lead to new capabilities in UAS detection in high clutter (urban and highly built environments like downtown areas) which is increasingly relevant for modern anti-terrorist operations. Results for this ongoing research will be reported when available.

#### VI. CONCLUSION

The paper has summarized our work on hardware, physics-aware signal processing, and machine learning for surveillance radar designed to detect and classify micro-UAS. Promising over-the-air UAS detection results have been obtained using SCF for feature extraction and a DBN for classification. Future work will focus on i) improved multi-directional situational awareness by using uniform circular arrays and lenses; and ii) using polyspectrum-based DSP (PDSP) methods to model the nonlinear phase modulation processes present in the rotational micro-Doppler signatures generated by UAS.

#### REFERENCES

- [1] M. Mozaffari *et al.*, "Beyond 5G with UAVs: Foundations of a 3D wireless cellular network," *IEEE Transactions on Wireless Communications*, vol. 18, no. 1, pp. 357–372, 2018.
- [2] A. Fotouhi et al., "Survey on UAV cellular communications: Practical aspects, standardization advancements, regulation, and security challenges," *IEEE Communications Surveys & Tutorials*, vol. 21, no. 4, pp. 3417–3442, 2019.
- [3] B. Li et al., "UAV communications for 5G and beyond: Recent advances and future trends," *IEEE Internet of Things Journal*, vol. 6, no. 2, pp. 2241–2263, 2018.
- [4] H. Shakhatreh et al., "Unmanned aerial vehicles (UAVs): A survey on civil applications and key research challenges," *IEEE Access*, vol. 7, pp. 48 572–48 634, 2019.
- [5] https://www.cbsnews.com/news/drone-over-white-house-sparks-new-security-concerns/.
- [6] http://www.bbc.com/news/world-europe-31619099.
- [7] https://arstechnica.com/information-technology/2013/09/germanchancellors-drone-attack-shows-the-threat-of-weaponized-uavs/.
- [8] https://techcrunch.com/2019/09/27/last-years-gatwick-drone-attack-involved-at-least-two-drones-say-police/.
- [9] I. Bisio et al., "Unauthorized amateur UAV detection based on WiFi statistical fingerprint analysis," *IEEE Communications Magazine*, vol. 56, no. 4, pp. 106–111, 2018.
- [10] P. Nguyen et al., "Matthan: Drone presence detection by identifying physical signatures in the drone's RF communication," in Proceedings of the 15th Annual International Conference on Mobile Systems, Applications, and Services, 2017, pp. 211–224.
- [11] C. Aker and S. Kalkan, "Using deep networks for drone detection," in 2017 14th IEEE International Conference on Advanced Video and Signal Based Surveillance (AVSS). IEEE, 2017, pp. 1–6.
- [12] C. Craye and S. Ardjoune, "Spatio-temporal semantic segmentation for drone detection," in 2019 16th IEEE International Conference on Advanced Video and Signal Based Surveillance (AVSS). IEEE, 2019, pp. 1–5.
- [13] H. Liu et al., "Drone detection based on an audio-assisted camera array," in 2017 IEEE Third International Conference on Multimedia Big Data (BigMM). IEEE, 2017, pp. 402–406.
- [14] A. Bernardini et al., "Drone detection by acoustic signature identification," Electronic Imaging, vol. 2017, no. 10, pp. 60–64, 2017.
- [15] D.-H. Shin et al., "A distributed FMCW radar system based on fiber-optic links for small drone detection," *IEEE Transactions on Instrumentation and Measurement*, vol. 66, no. 2, pp. 340–347, 2016.
- [16] H. Sun et al., "Improving the Doppler resolution of ground-based surveillance radar for drone detection," *IEEE Transactions on Aerospace* and Electronic Systems, vol. 55, no. 6, pp. 3667–3673, 2019.
- [17] G. J. Mendis et al., "Deep learning based Doppler radar for micro UAS detection and classification," in MILCOM 2016 - 2016 IEEE Military Communications Conference, Nov 2016, pp. 924–929.

- [18] G. J. Mendis et al, "Deep learning cognitive radar for micro UAS detection and classification," in Cognitive Communications for Aerospace Applications Workshop (CCAA), 2017. IEEE, 2017, pp. 1–
- [19] G. J. Mendis et al., "Deep Learning Based Radio-Signal Identification With Hardware Design," *IEEE Transactions on Aerospace and Electronic Systems*, vol. 55, no. 5, pp. 2516–2531, 2019.
- [20] T. D. Randeny, "Multi-Dimensional Digital Signal Processing in Radar Signature Extraction," Ph.D. dissertation, University of Akron, 2015.
- [21] W. A. Gardner et al., "Cyclostationarity: Half a century of research," Signal Processing, vol. 86, no. 4, pp. 639 697, 2006. [Online]. Available: http://www.sciencedirect.com/science/article/pii/S0165168405002409
- [22] G. Hinton et al., "A fast learning algorithm for deep belief nets," Neural Computation, vol. 18, pp. 1527–1554, 2006.
- [23] A. Fischer and C. Igel, "An Introduction to Restricted Boltzmann Machines," L. Alvarez et al. (Eds.): CIARP 2012, LNCS, vol. 7441, pp. 14–36, 2012.
- [24] G. E. Hinton, "Training products of experts by minimizing contrastive divergence," *Neural computation*, vol. 14, no. 8, pp. 1771–1800, 2002.
- [25] K. Swersky et al., "A tutorial on stochastic approximation algorithms for training restricted Boltzmann machines and deep belief nets," in 2010 Information Theory and Applications Workshop (ITA). IEEE, 2010, pp. 1–10.
- [26] M. A. Carreira-Perpignan and G. Hinton, "On Contrastive Divergence learning," Artificial Intelligence and Statistics, 2005.
- [27] K. H. Cho et al., "Gaussian-Bernoulli deep Boltzmann machine," in Neural Networks (IJCNN), The 2013 International Joint Conference on, Aug 2013, pp. 1–7.
- [28] S. Marsland, Machine Learning: An Algorithmic Perspective, Second Edition (Chapman & Hall/Crc Machine Learning & Pattern Recognition). Chapman and Hall/CRC, 2014.
- [29] C. A. Balanis, Antenna theory: analysis and design. John Wiley & Sons, 2016.
- [30] P. Ioannides and C. A. Balanis, "Uniform circular and rectangular arrays for adaptive beamforming applications," *IEEE Antennas and Wireless Propagation Letters*, vol. 4, pp. 351–354, 2005.
- [31] CASPER, "Reconfigurable open architecture computing hardware (ROACH-2) FPGA platform." Oct. 2013 (accessed February, 2018), Available: https://casper.berkeley.edu/wiki/ROACH-2Revision2.
- [32] S. Pulipati et al., "Design of 28 GHz 64-QAM digital receiver," in 2019 International Workshop on Antenna Technology (iWAT), 2019, pp. 193– 196.
- [33] S. Pulipati et al., "A Direct-Conversion Digital Beamforming Array Receiver with 800 MHz Channel Bandwidth at 28 GHz using Xilinx RF SoC," in 2019 IEEE International Conference on Microwaves, Antennas, Communications and Electronic Systems (COMCAS). IEEE, 2019, pp. 1–5.
- [34] D. R. Brillinger, "An introduction to polyspectra," The Annals of mathematical statistics, pp. 1351–1374, 1965.
- [35] C. P. Silva et al., "Application of polyspectral techniques to nonlinear modeling and compensation," in 2001 IEEE MTT-S International Microwave Sympsoium Digest (Cat. No. 01CH37157), vol. 1. IEEE, 2001, pp. 13–16.
- [36] J. K. Tugnait, "Detection of non-Gaussian signals using integrated polyspectrum," *IEEE Transactions on Signal Processing*, vol. 42, no. 11, pp. 3137–3149, 1994.
- [37] C. L. Nikias and M. R. Raghuveer, "Bispectrum estimation: A digital signal processing framework," *Proceedings of the IEEE*, vol. 75, no. 7, pp. 869–891, July 1987.